Journal of Seismology **3:** 177–190, 1999.

Tomographic imaging of P- and S-wave velocity structure beneath Costa Rica

Z. S. Yao, R. Quintero & R. G. Roberts
Department of Earth Sciences, Uppsala University, Villavagen 16, 752 36 Uppsala, Sweden

Received 21 January 1998; accepted in revised form 11 September 1998

Key words: travel time tomography, Costa Rica

Abstract

45287 P-wave and 26813 S-wave arrival times from the data base of the Costa Rica network have been tomographically inverted to image the structure beneath Costa Rica. A regularized recursive least squares inverse method was used to produce the high resolution and minimum variance model parameter estimates. The first arrival times are calculated using a finite difference technique, which allows for flexible parameterization of the velocity model and easy inclusion of topography and source-receiver geometry. The P wave velocity structure and hypocenters are determined simultaneously, while the S wave velocity structure is determined using the relocated seismicity and an initial model derived from the P wave model assuming an average P to S wave velocity ratio of 1.78. The most prominent features in the inverted model are a low velocity structure under the volcanic chain in the center of the country, which is related to the hot material connected with the active volcanoes; and a high velocity zone in the mantle, which is related to the Cocos plate subducted under Costa Rica.

Introduction

Costa Rica is located in a complex tectonically active region, where the Cocos plate is subducting below the western margin of the Caribbean plate under Central America. The collision of the plates together with the interaction with the Nazca plate and the Panama block make Costa Rica one of the highest seismicity regions in the world.

Since 1984, the Costa Rica Volcanological and Seismological Observatory of the Universidad Nacional (OVSICORI-UNA), together with the University of California, Santa Cruz, has been operating a permanent short period seismic network, and thousands of earthquakes have been recorded. The recorded earthquake hypocenters are distributed throughout the entire area down to 40 km and then along the subduction zone down to 200 km, which makes this region very suitable for seismic tomograph y studies.

Deduced velocity structures are often used to image the tectonic regime of an area and therefore to test models of geological evolution (De Jonge et al., 1993). Three dimensional seismic velocity images through seismic tomography may also reveal the existence of heterogeneity in volcanic zones, earthquake faults, subduction zones and other diverse geological structures, which can help us understand deeper structures.

The P wave velocity structure in northern Costa Rica has been studied by Matumoto et al. (1977) and by Liaw (1981) using simple 1D (layered) models. Recently, Protti et al. (1996) selected over 1300 events from the catalogue of the Costa Rica network to simultaneously invert for the location and three dimensional P-wave crustal velocity structure of central Costa Rica. Their results show a correlation between velocity structure and tectonic features. However, the resolution is limited to the crust with a thickness of up to 30 km; Quintero et al. (1997) selected 2967 events from the catalogue to invert the 3D P and S wave velocity distributions in the central part of Costa Rica down to a depth of 60 km.

In this study, many more events have been used to study the velocity structure of the whole of the Costa

Rica area down to 100 km, and both P and S wave first arrivals are used. The method used is based on regularized recursive Least Squares, which allows us to solve the whole equation system equation by equation. The advantage of this technique is that we can handle the inversion of large matrices very effectively.

Data and model configuration

Our study area is 400×200 km^2 and covers the whole of Costa Rica on the surface. The purpose of our study is to reveal velocity structure down to 100 km, but the depth of the model is down to 140 km in order to obtain more ray penetration through the study area. We choose an x axis in the direction parallel to Middle America Trench. The coordinate system for our study is shown in Figure 1. The network contains 24 stations with short period seismometers that are very densely distributed in the central part of the area (Figure 2). We carefully selected data from the period 1984 to 1991. All the events were relocated using the program HYPOINVERSE (Klein, 1978, 1984) and the 1D P wave velocity structure model shown in Figure 4. Part of the data set is coincident with the recent crustal 3D velocity study by Protti (1996). The selection of earthquakes for the present study is based on the following criteria: (1) The earthquake occurred in the study area; (2) P arrivals were recorded by at least 7 stations and both P and S arrival time are clearly picked; (3) estimated location errors are less than 3 km for horizontal and 5 km for vertical coordinates, to make sure that the locations of all the selected events are well controlled by the network. In total, 5073 earthquakes were selected in this study. The locations of the earthquakes selected in our study are shown in Figure 3. From these events, 45287 P-wave and 26813 S-wave arrival times were picked.

The study area was divided into 10 layers. The thickness chosen for each layer is 10 km for the first 6 layers and 20 km for the remaining four layers because we have less ray coverage in the deep layers. These layer thicknesses were chosen partly because they represent a compromise between the model used for relocation and the model given by Matumoto et al. (1977). Within each layer, the model is further discreted into 20×20 cells (in the x and y directions) and the geographical size of each cell is 20×10 km^2. The total number of blocks in the model is thus 4000. Assuming the velocity within each block is constant, we invert for the P and S wave velocity for each block. Inversions of P and S wave first arrival data were carried out separately. The starting model for the P wave inversion was a one dimensional velocity model interpolated from the relocation model. The initial model for S wave inversion was derived from the results of the P wave inversion using a P wave to S wave ratio of 1.78 as suggested by the recent work of Quintero et al. (1997).

Method description

The travel time of a seismic wave generated by an earthquake is a nonlinear function of the station coordinates ($\mathbf{x}_r$), the hypocentral parameters ($\mathbf{x}_s$) and the velocity field ($\mathbf{m}$).

$$t^{\text{obs}} = f(\mathbf{x}_r, \mathbf{x}_s, \mathbf{m}). \tag{1}$$

In general, neither the true hypocentral parameters nor the velocity field are known. Therefore, Equation (1) can not be solved directly because only arrival times and station coordinates are measurable. Instead of solving Equation (1) directly, we linearize the equation by applying a Taylor expansion to (1) with respected to the parameters describing both hypocenters and velocity field. If the parameters are close to the true values, we can keep only the first order term of the series to obtain a linear relationship between the travel time residual and adjustments to the hypocentral ($\Delta\mathbf{x_s}$) and velocity ($\Delta\mathbf{m}$) parameters:

$$t^{\text{res}} = t^{\text{obs}} - t^{\text{cal}} \simeq \frac{\partial f}{\partial \mathbf{x_s}} \Delta\mathbf{x_s} + \frac{\partial f}{\partial \mathbf{m}} \Delta\mathbf{m}, \tag{2}$$

where t^{cal} represents the theoretical arrival times in the reference velocity model. In matrix notation, Equation (2) can be written as

$$\Delta\mathbf{T} = \mathbf{A}\Delta\mathbf{X}, \tag{3}$$

where $\Delta\mathbf{T}$ is the vector of arrival time residuals, $\mathbf{A}$ is the matrix composed of partial derivatives of travel times with respect to both model and hypocentral parameters. $\Delta\mathbf{X}$ is the vector of both model and hypocentral parameter perturbations. Equation (3) describes the coupled hypocenter-velocity model parameters relation and it can be separated into two equation systems, i.e., one containing the hypocenter information and the other containing the velocity model parameter information (following Pavlis and Booker, 1980). The equation system pertaining to the velocity model is then written as

$$\mathbf{Y} = \mathbf{G}\Delta\mathbf{m}, \tag{4}$$

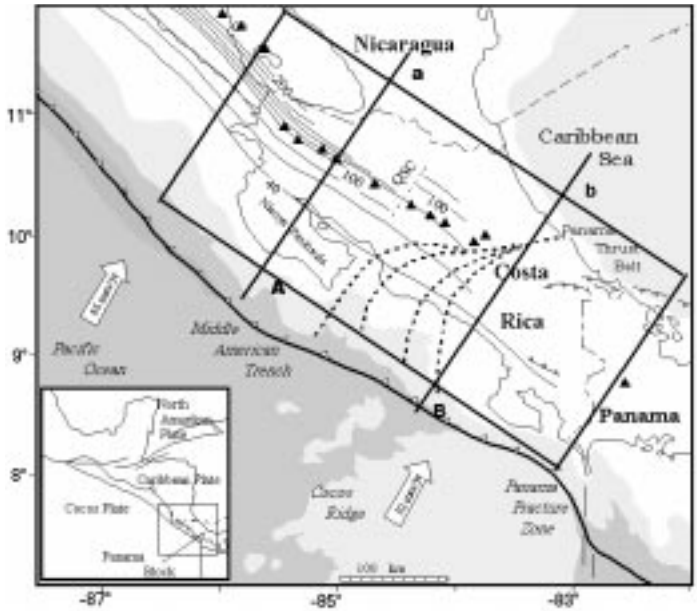

Figure 1. Tecnotic setting of southern Central America. Solid contours indicate the geometry of the top of the Wadati–Benioff zone from Protti et al. (1994). Triangles are active volcanoes. Convergence velocities between Cocos and Caribbean plates were computed from DeMets et al. (1990). QSC: Quesada sharp contortion. Insert: major plate boundaries in Central America and location of large-scale map. Dashed lines across central Costa Rica schematically represent the shear zone that marks the boundary between the Caribbean plate and the Panama block. The location of the study area is shown by the rectangle. Lines A-a and B-b indicate the locations for vertical cross section studies.

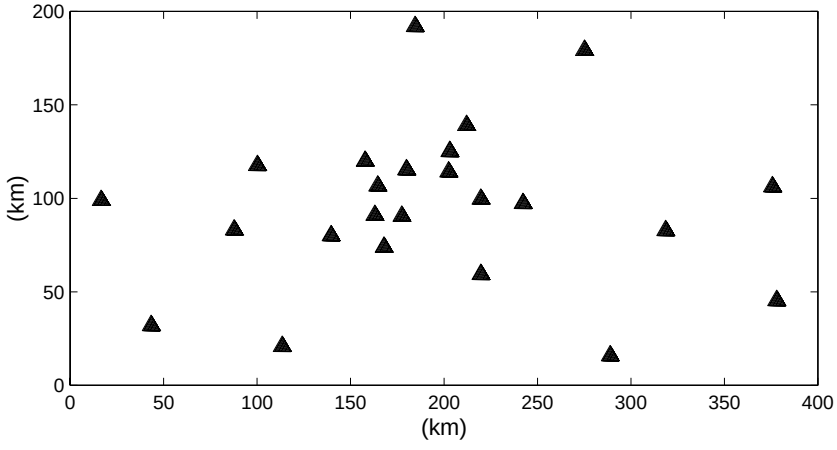

Figure 2. The distribution of the stations.

where **Y** and **G** are the altered residual vector and velocity derivative matrix.

The solution of (4) can be written as (e.g., Tarantola, 1987)

$$\hat{\mathbf{m}} = \mathbf{m}_0 + \mathbf{C}_0\mathbf{G}^T(\mathbf{G}\mathbf{C}_0\mathbf{G}^T + \mathbf{D})^{-1}(\mathbf{Y} - \mathbf{G}\mathbf{m}_0), \quad (5)$$

$$\mathbf{C} = \mathbf{C}_0 - \mathbf{C}_0\mathbf{G}^T(\mathbf{G}\mathbf{C}_0\mathbf{G}^T + \mathbf{D})^{-1}\mathbf{G}\mathbf{C}_0, \quad (6)$$

where $\mathbf{m}_0$ is an a priori model parameter vector, $\mathbf{C}_0$ is the corresponding a priori covariance matrix and **C** is an a posteriori covariance matrix.

If we interprete the $\mathbf{m}_0$ and $\mathbf{C}_0$ in (4) as the model parameters and their covariance estimated from an assumed previous data set, then **m** is the solution of the whole data set, i.e., the data set we have and the data set we assumed. Based on this idea, we can re-write (4) in recursive form (e.g., Yao et al., 1998)

$$\hat{\mathbf{m}}(n+1) = \hat{\mathbf{m}}(n) + \mathbf{k}(n+1)\times \\ \times(y(n+1) - \mathbf{g}(n+1)\hat{\mathbf{m}}(n)), \quad (7)$$

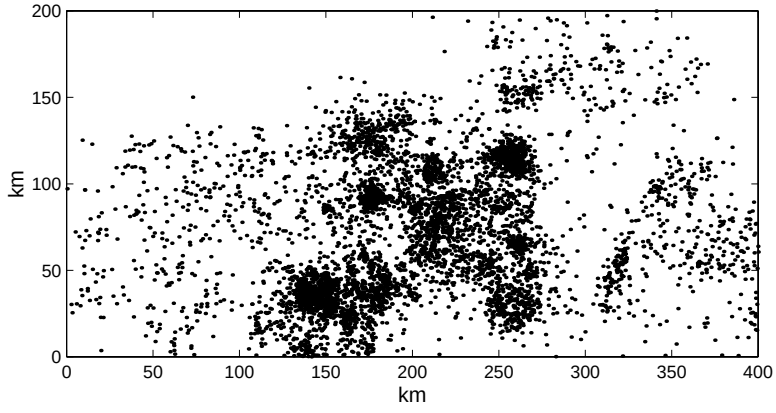

Figure 3. The distribution of the epicenters selected in this study.

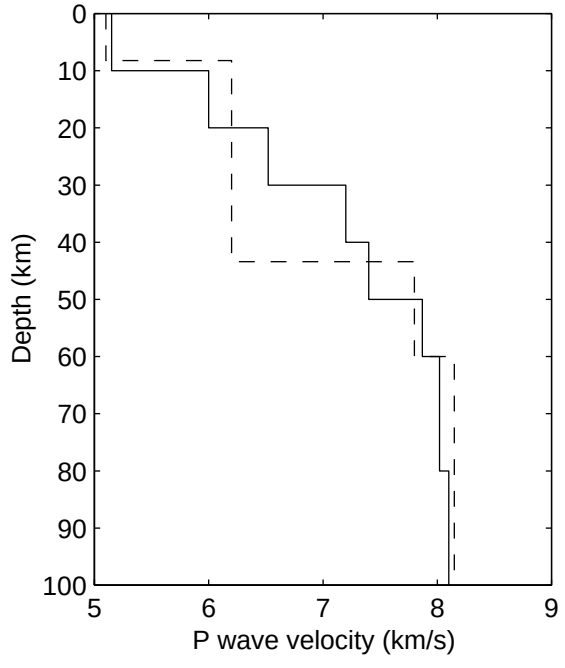

Figure 4. The 1-D P wave velocity model for HYPOINVERSE (dash line) and the 'Mimimum 1-D model' (solid line).

where $\mathbf{k}(n+1)$ is defined as follows:

$$\mathbf{k}(n+1) = [\mathbf{g}(n+1)\mathbf{C}(n)\mathbf{g}^T(n+1)+ \\ +d(n+1)]^{-1}\mathbf{C}(n)\mathbf{g}^T(n+1) \qquad (8)$$

and

$$\mathbf{C}(n+1) = [\mathbf{I} - \mathbf{k}(n+1)\mathbf{g}(n+1)]\mathbf{C}(n). \qquad (9)$$

With this recursive Equation (7–9), a very large equation system can be solved equation by equation, i.e., this is a row action method. Comparing with full matrix inverse techniques the advantage of this method is that it can reduce both computer time and the computational memory required (Yao et al., 1997). In practice, the a priori covariance matrix can also taken as regularization, or constraining, equations introduced into Equation (3) (e.g., Spakman, 1993). Regularization is often used to minimize artifacts due to model parameterization and solution instability (e.g., Berryman, 1990; Lees and Crosson, 1989; Benz et al., 1996). Regularization through a Gaussian function, which constrains the velocity model through a correlation length, has often been used in 3D velocity structure studies (e.g., Tarantola and Valette, 1982; Yanick, 1996). Here, we use the modified Gaussian function to construct the a priori covariance matrix $\mathbf{C}_0$:

$$\left[C(0)_{i,j}\right] = (\Delta_{\mathbf{m}})^2 \left[\sigma(\mathbf{r}_i)\sigma(\mathbf{r}_j)\exp\left(-\frac{(\mathbf{r}_i - \mathbf{r}_j)^2}{\Delta_0^2}\right)\right] \qquad (10)$$

where $\Delta_{\mathbf{m}}$ is a constant representing the standard deviation of $\mathbf{m}_0$, $\mathbf{r}_i$ are position vectors in the model space and Δ_L is a correlation length that controls the smoothness of the inverted model. $\sigma(\mathbf{r})$ is a weighting factor that can be chosen from a priori knowledge. Here, we simply chose it as a ray coverage function (the ray density in sampled cells) so that higher resolution can be obtained in volumes where the ray coverage is denser. In fact, this regularization is conceptually similar to using coarser blocks in our model where there is less ray coverage (Yao et al., 1998).

During the process of solving equations recursively, the covariance matrix, i.e., an a posteriori covariance matrix, is a by-product. With this covariance, we can write the resolution matrix as (e.g., Tarantola, 1987)

$$\mathbf{R} = \mathbf{C}\mathbf{G}^T\mathbf{D}^{-1}\mathbf{G} = \mathbf{I} - \mathbf{C}\mathbf{C}_0^{-1}, \quad (11)$$

where $\mathbf{C}$ is the final a posteriori covariance matrix from the last step of the recursive calculation.

Finite difference forward calculation

The accurate and efficient forward calculation of the traveltime based on the model is an important stage in tomography. Traditionally, ray shooting (e.g., Benz and Smith, 1984) and approximate ray-bending (e.g., Thurber, 1984) techniques have been used to calculate traveltimes in smoothly varying two and three dimensional velocity structures. While relatively efficient, these techniques have difficulty in finding the least-time path in complex velocity structures and fail at caustics. In this study, finite difference solving of the Eikonal equation was chosen to calculate the first arrival times. This method was initially developed for two dimensions (Vidale, 1988), and then the scheme was extended to three dimensions (Vidale, 1991; Podvin and Lecomte, 1991). The great advantage of the technique is that it explicitly solves for transmitted and diffracted body waves in structures with large velocity contrasts and arbitrary shape. The formulation of the travel-time tomographic inversion requires knowledge of the ray paths because the matrix containing ray lengths within each cell needs to be constructed. However, this knowledge is not explicitly produced by the finite difference computation. Therefore, the back tracing technique was employed to trace the ray trajectory, i.e., back tracing perpendicular to the wave front (the steepest path) from the source to the receiver. Using finite-difference forward modeling for two- and three-dimension inversion has been discussed in various articles, (e.g., Ammon and Vidale, 1993; Hole, 1992) and is a robust technique for the computation of first arrival times in complex velocity structures and with extreme topography (e.g., Benz et al., 1996). Therefore, it is well suited for this study because of the expected large velocity contrasts in the vicinity of the subduction slab. In order to achieve accurate travel time calculations, the grid spacing used for the travel time calculations is not the same as that to be used for the velocity image reconstruction. In fact, the arrival time calculations are usually done on a smaller grid spacing (e.g., Benz et al., 1996). In this study we use a uniform horizontal and vertical grid spacing of 1 km for arrival time and ray tracing calculations. After each iteration in the inversion the velocities from the larger grid spacing used for the inversion are linearly interpolated onto the smaller grid spacing before computing the arrival times. With the one dimension velocity starting model, results of finite difference travel time calculations were compared with the analytic solution, which shows that with such grid spacing, the error can be controlled within 0.02s, which is very small compared to the estimated standard deviation of the P wave picking error.

Inverse process

Since the solution to the local earthquake tomography problem is based on iterative refinement of a linearized approximation to a nonlinear function, i.e., solutions are obtained by linearization with respect to a reference Earth model, the resulting tomographic images may be dependent on the initial reference models and hypocenter locations (Micheal, 1988; Van der Hilst and Spakman, 1989; Van der Hilst et al., 1991). An inappropriate initial reference model can affect the quality of the 3D image by introducing artifacts and may also lead to underestimation of the uncertainties of the results (Kissling et al., 1994). The chances for successful estimation of the true model can be improved by selecting a starting model in the neighborhood of the true model. However, how to find such an initial model is very much dependent on the available a priori knowledge of the velocity structure. Unfortunately, prior information about the velocity structure is not always accessible. In our case only the few velocity structure studies mentioned above have been carried out in this area and the previous results were limited to the crust. Therefore, we adopt the concept of the 'Minimum 1-D model' in our inversion. The concept of a 'Minimum 1-D model' was originally introduced by Crosson (1976) and has been discussed extensively by Kissling et al. (1994). According to Kissling's results (Kissling et al., 1984; Kissling, 1988; Kissling et al., 1994), a 3D model derived from this 'Minimum 1-D model' has minimal dependence on the reference model. Hence, our inverse scheme includes two stages: First, travel time data are jointly inverted to obtain a 1D tomographic solution, i.e., the 'Minimum 1-D model', together with revised hypocenters. Second, the 3D tomographic inversion for velocity structure is carried out by using the minimum 1D model as the initial model.

The results show that the P wave minimum 1D model is close to the model used for event location (see

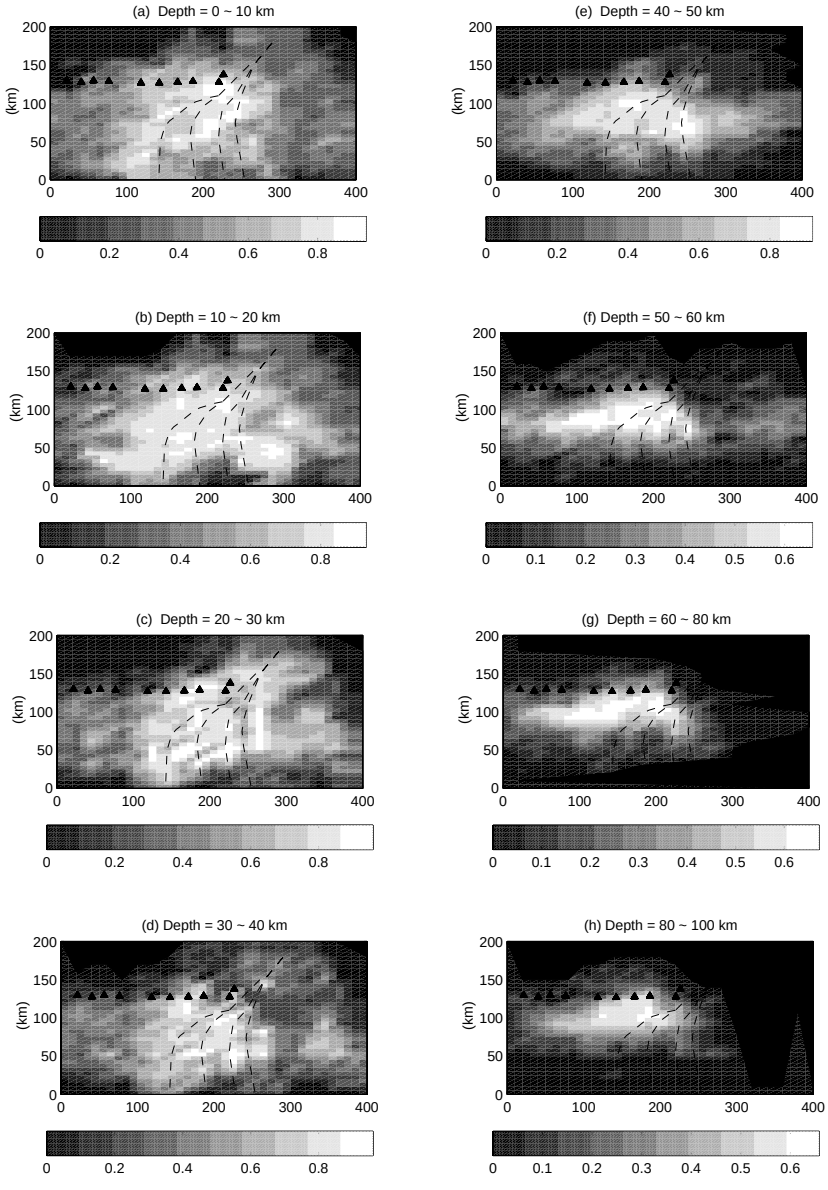

Figure 5. Distribution of diagonal element resolution for the inverted model from P arrivals.

Figure 4). It should be stressed that the 'Minimum 1-D model' for P velocity obtained from this stage is itself a least squares solution with a few model parameters and this 1D model may present a reliable average model of the true 3D P velocity model at the given depths. Therefore, with this we can also check the possible sources of systematic errors, such as mislocation of stations and timing problems, in the selected data. In order to check these possible sources of systematic errors, the distributions of P travel-time residuals (observed minus calculated) for each receiver are plotted out. The residuals appear to be approximately normally distributed and the rms of the residuals are less than 0.45s at all stations. The means of the residuals are between –0.25s to 0.25s with the stations located on the volcanic area tending to show positive mean values.

The minimum 1D model for S waves is derived directly from P wave to S wave velocity ratio of 1.78 (Quintero et al., 1997). With the minimum 1D models the rms of the travel time residuals is reduced from

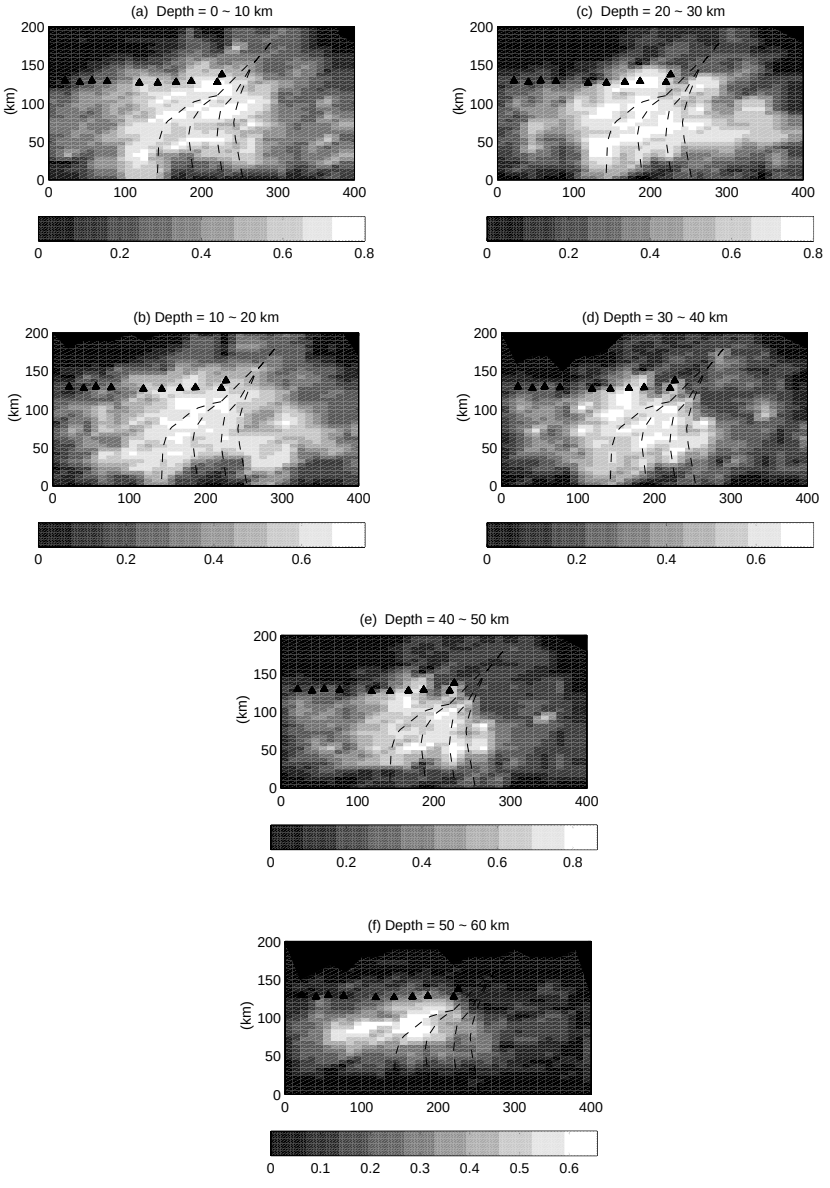

Figure 6. Distribution of diagonal element resolution for the inverted model from S arrivals.

0.55s in the starting model to 0.41s for P wave arrivals and from 0.61s to 0.48s for S arrivals.

Starting from the minimum 1D models, we iteratively calculated the final three dimensional model perturbations to the minimum 1D model for P and S waves, respectively. For P waves, we simultaneously update the hypocenters, ray paths and travel times at each iteration step to obtain the 3D P wave velocity structure and the updated hypocenters. For S waves, the hypocenters were taken from the results of P wave inversion and were not updated any more. After 6 iterations for P wave inversion, further variance reduction was negligible. The final rms was 0.25s. For S-wave inversion, 4 iterations were used to obtain the final rms of 0.39s.

Results and their tectonic implications

Resolution analysis

Before presenting the obtained results, we first show the distribution of the diagonal elements of the resolution matrices for the images for both P and S waves

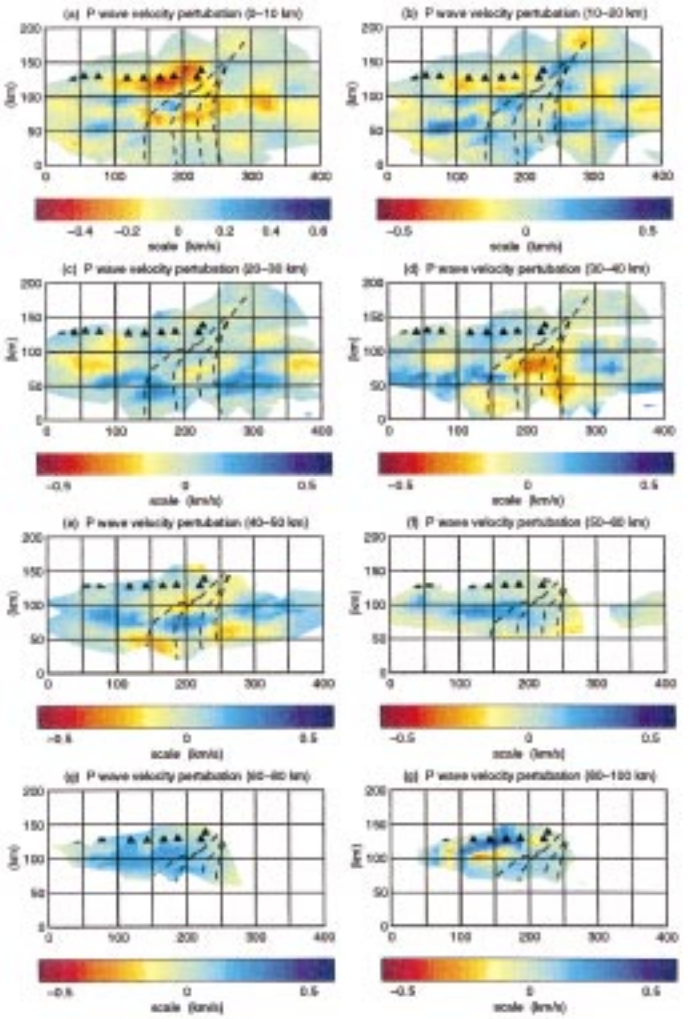

Figure 7.

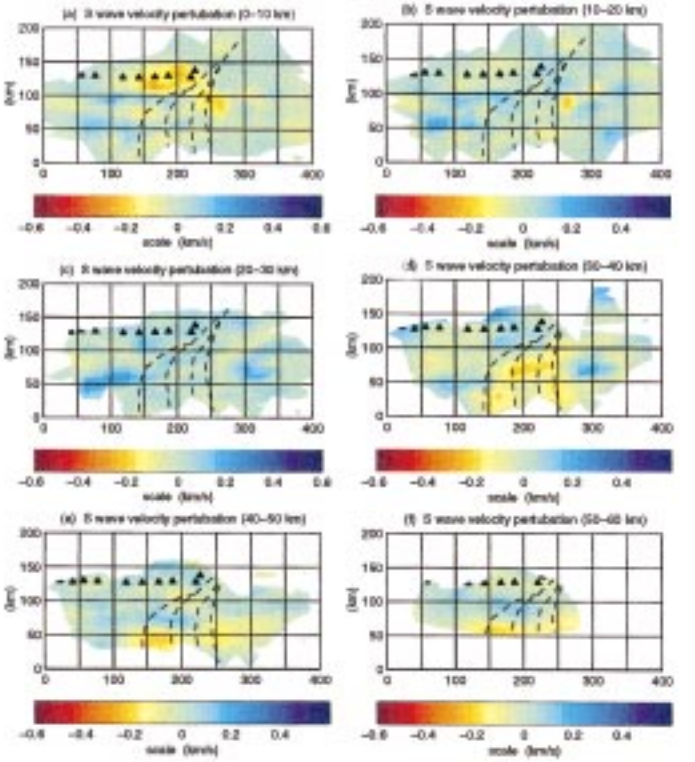

Figure 8.

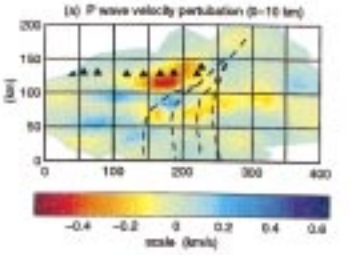

Figure 9.

←

Figure 7: Tomographic result for P wave velocity perturbation from the 1D minimum P wave velocity model.
Figure 8: Tomographic result for S wave velocity perturbation from the 1D minimum S wave velocity model.
Figure 9: The tomographic result by LSQR for P wave velocity perturbation from the 1D minimum P wave velocity model in the first layer.

(Figures 5 and 6). The values of diagonal elements of the resolution matrix, which are not only dependent on how many rays pass through each block (known as the hit count), but mainly on the geometries of the rays passing though the block, provide a measurement of the quality of the images. In general, the higher the value is, the more reliable the image. In order to get a quantitative understanding about the relationship between the diagonal element values and the qualities of the images, synthetic data with the real observation system and a checkboard model have been used in resolution analysis. We conclude that results where the diagonal elements of the resolution matrices are less than 0.3, are unreliable for this study.

Errors due to mislocation analysis

Because the local earthquake tomographic inversion is used to solve the equation with coupled hypocenter and velocity model parameters, any errors in hypocenter location can transfer to the inverted velocity structure. To judge the location accuracy, we compared the final hypocenters after 3D inversion with that used in the initial model, i.e., 'the minimum 1D models'. The change in position of those hypocenters (distance) is not large, on average 1.2 km for depths of 0–40 km, 1.8 km for depths of 40–60 km and 2.7 km for depths of 60–100 km. We believe that these values give a meaningful indication of the location errors. These errors may affect both the travel time calculations and ray path tracing. In order to check how such errors may affect the results, synthetic data generated from the final hypocenters and the station distributions were inverted with both initial and final hypocenter distributions. The main purpose of the test is to see to what extent the model of the main feature, i.e., the subduction zone in the area, may be affected by event mislocations. The results show that the effects were small, which may be because compared to the size of the blocks of the model, the changes of the hypocenters are not significant.

Velocity perturbations and their tectonic implications

To see the correlation between the tomography structure and tectonics, simplified geologic features are also shown in Figure 1. A more detailed description of the regional geology of Costa Rica can be found in the papers by Protti (1994, 1996). Subduction of the Cocos plate under Costa Rica dominates the study area. The subduction increases from 86 mm/year in the north to 95 mm/year in the south of Costa Rica (DeMets et al., 1990). As a result of this subduction process, an active volcanic chain runs through central Costa Rica. Based on the results of seismicity studies, the subducting slab is believed to be segmentated under central Costa Rica, i.e., the Quesada Sharp Contortion (QSC) (e.g. Protti, 1994). North–west of the QSC the subducted slab is older and dips more steeply than in the south–east. The shallow subduction of young oceanic lithosphere in southern Costa Rica hinders active volcanics. A wide fan shaped shear zone marking the boundary between the Caribbean and the Panama block crosses central Costa Rica (see Protti et al., 1996).

Figures 7 and 8 show the tomographic results as velocity perturbations with respect to the 'minimum 1D model' as deduced from both P and S travel times. The places where the corresponding elements of the diagonal resolution matrix are less than 0.3 are shown in white. Because of the relatively sparse samping in deep layers for S waves, the velocity images for the S wave model is only down to 60 km in depth.

Upper crust (0–20 km)

One of most prominent features for both P and S wave velocity in the upper crust is the lower velocity zone centered on the volcanic area (Figure 7(a), (b) and Figure 8(a), (b)). These low velocities might be expected for the warm material under the active volcanic chain, as, e.g., in northern Honshu, Japan (Zhao et al., 1992), Kilauea, Hawaii (Thurber, 1984) and Redoubt, Alaska (Benz et al., 1996).

In Figure 7(a), low velocity areas are found at the coordinates x–210 km, y–70 km and at x from 230 to 400 km, y–90 km, which are located in the Coronado Basin and Teraha Basin, respectively. The sedimentary basins in these regions are composed of over 5 km of marine sediments (Rivier, 1985; Ponce and Case, 1987). This low velocity pattern is seen only weakly in the second layer (Figure 7(b)), which indicates that the low velocities are largely at shallow depth and are related to the sediments. Corresponding

velocity perturbations are also seen in Figure 8(a), (b) (S waves).

In the first layer, anomalously high P wave velocities are mostly in the north–west of the study area, i.e., the coordinates of *x* are from 50 to 200 km and *y* from 40 to 100 km in Figure 7(a). These high velocities may indicate high density materials and are consistent with the relatively high positive Bouguer anomalies observed in this area (Figure 10). In fact, the high velocity centered at *x* 80 km and *y* 50 km is located in an area with dense oceanic crustal rock (late Jurassic to early Tertiary), and the high velocity centered at *x* 70 and *y* 60 km is located in an area with mesozoic ophiolitic rocks (see Ludington et al., 1987). The same feature can be seen in S wave velocity images (Figure 8(a), (b)). High velocities are also seen in other places in the second layer of the P wave image (Figure 7(b)). One of them is around *x* coordinate 250 km with *y* coordinates from 100 to 150 km and it forms a clearly contrasting velocity structure with the low velocity of the volcanic chain. Another high velocity region is located at *x* coordinate between 280 to 300 km with *y* coordinate about 50 km.

Lower crust (20–40 km)

The images from P and S waves in the lower crust are very similar (Figures 7(c), (d) and 8(c), (d)). The low velocity perturbation beneath the volcanic chain is no longer clearly seen. This is in agreement with the previous study by Protti et al. (1996). Similar shallow low velocity zones under active volcanoes have been found by others in different areas (e.g., Thurber, 1984; Zhao et al., 1992; Benz et al., 1992), and may be a common phenomenon for such structures.

Within the shear zone, anomalously low velocities can be seen in both P wave and S wave images. These low velocities increase from the third layer to the fourth layer. The low velocity distributions may correspond to the Costa Rica Transcurrent Fault Zone (Astorga et al., 1991; Escalante and Astorga, 1994) that is characterized by complex tectonic features displaying predominantly strike-slip displacements (Montero and Dewey, 1982; Alvarado et al., 1986; Barpuero and Rojas, 1994).

The high velocity perturbation for both P and S waves at *x* from 70 to 180 km and *y* about 50 km in layer three (Figure 7(c) and Figure 8(c)) may be the continuation of a structure from the the layer above. However, it is prolonged and enhanced in the fourth layer, which may indicate that the major contribution to the positive Bouguer anomaly (Figure 9) is from high velocity material in the deep crust.

Centered at *x* 70 km, *y* 80 km, low velocity perturbations can be found for the P velocity (Figure 7(c) and 7(d)). Very weak corresponding low velocity perturbations are seen for S velocity (Figure 8(c) and 8(d)). This indicates a low ratio of P to S velocity. The same pattern can also be seen in the middle of the right side of Figure 7(c) and 8(c), where the active volcanoes occur.

In Figure 7(d) and 8(d) the high velocity along the *x* direction with *y* axis about 50 km could be related to the subducting plate. These high velocities are broken by the low velocity area in the central part. This may reflect the change of the geometry of the subducting slab.

Upper mantle (40–60 km)

The main features are similar for both P and S wave images of the upper mantle. S wave images show a more smooth pattern because the resolution is not as good as for the P wave data and more smoothing is necessary in the inversion. In layer 5 between *y* coordinates 50 and 100 km, a clear long positive velocity perturbation belt parallel to the *x* axis can be seen in the P wave image (Figure 7(e)). This high velocity belt has a curvature that is similar to that of the trench. It may reflect the shape of the cooler oceanic Cocos plate as it plunges beneath Costa Rica at this depth. Such a high velocity belt is not seen clearly in the S wave image at this depth (Figure 8(e)), but it can be traced. There are also low velocity perturbation areas distributed in both P and S wave images.

The high P wave velocity belt in layer 5 changes dramatically as we move down to layer 6. In layer 6, this belt is segmentated into two parts. The north part has nearly the same maximum magnitude of perturbation relative to the reference model as that of the layer above, but a little bit further away from the trench. To the S–E, the feature is much weaker, which may indicate that the subducted plate is not present here. The less resolved part in the south part may also indicate that the geometry of the subducted plate is different from that in the N–W. Segmentation of subducted slabs at relatively shallow depth is a common feature. For instance, Isacks and Barazabgi (1977) investigated lateral segmentation along many subducted plates and concluded that segmentation is one of the important factors enabling more uniform bending of the plate along each segment. The changing characteristics of velocity can also be accounted for by the difference in

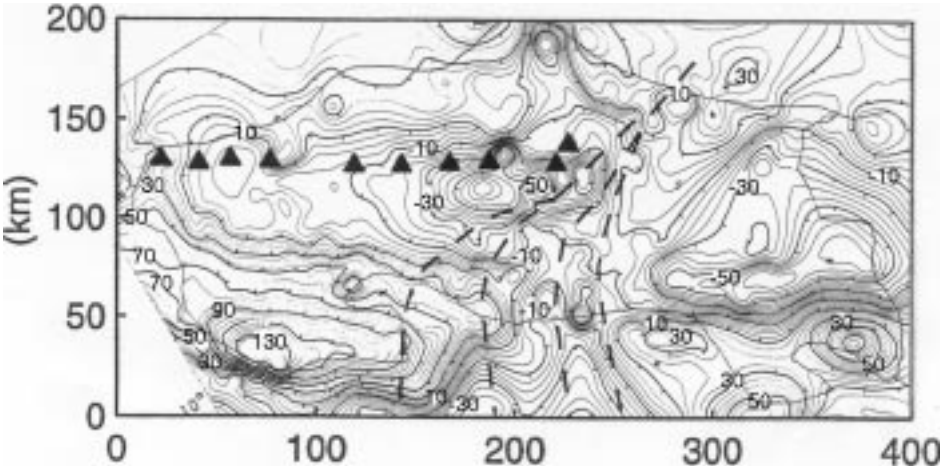

Figure 10. Bouguer anomalies (conturs in mGal) from Ponce and Case (1987).

age of the subduced plate. Protti et al. (1994) investigated the age of the subducted plate beneath this area and found that the ages of the plate in the north is older than that in the south by 5 Myr. The higher velocity in the northern part of the subducted plate than in southern part may indicate that an older, denser oceanic lithosphere is subducting beneath northern Costa Rica than beneath southern Costa Rica.

Between the two high velocity perturbations described above, there is a low velocity perturbation structure in the *y* direction, which is coincident with the shear zone and the Cocos Ridge. In layer 6, the S wave image shows also the high velocity perturbation corresponding to that of P, but only the N–W part is resolved (Figure 8(f)).

Deep mantle (60–100 km)

From a depth of 60 km, only the P wave images are resolvable (Figure 7(g), (h)). Because the events are concentrated in the subduction zone, the images are limited to the area around the subduction zone. The prominent feature is the elongated high velocity zone in the images. We believe that this high velocity structure corresponds to the subducted plate, which is relatively cool. Subducted plates with high velocities are also observed in many other places, e.g., in northern Honshu, Japan (Zhao et al., 1992).

Discussion and conclusion

Applying a regularized recursive least squares inversion method in combination with a finite difference travel time calculation technique, we deduced three-dimensional P and S wave velocity structures. The deduced distributions of P and S waves velocities show very similar patterns. In the crust, low velocity zones are found beneath the active volcanoes and this low velocity perturbation does not continue into the lower crust. An area of anomalously low velocity in the shear zone in the lower crust may reflect the transcurrent fault system that indicates the boundary between the Caribbean and Panama blocks. A high velocity area in the upper mantle related to the subducted Cocos plate has the same curvature as that of the trench. This high velocity area is segmented into two parts at a depth of 50 km and is shifted away from the trench by varying distances. This indicates that the subducted plates corresponding to these two parts have different geometries with a steeper angle (about 47°, Figure 11(a)) of subduction in the north than that (about 41°, Figure 11(b)) in the south.

Resolution analysis and synthetic data analysis indicate that all the tomographic images shown above are generally well resolved by our recursive least squares algorithm. However, our results have some differences from the previous 3D velocity study by Protti et al. (1996). For example, instead of a low velocity structure beneath the volcanic chain in our result, the low velocity related to the volcanic chain in the previous results is 30 km trenchward. Because Protti et al. used the inversion technique of Thurber (1984), a question naturally arises: are the results dependent on the method? In order to check this point, a LSQR method was used for comparison. The computer code for solving a linear equation system (3)

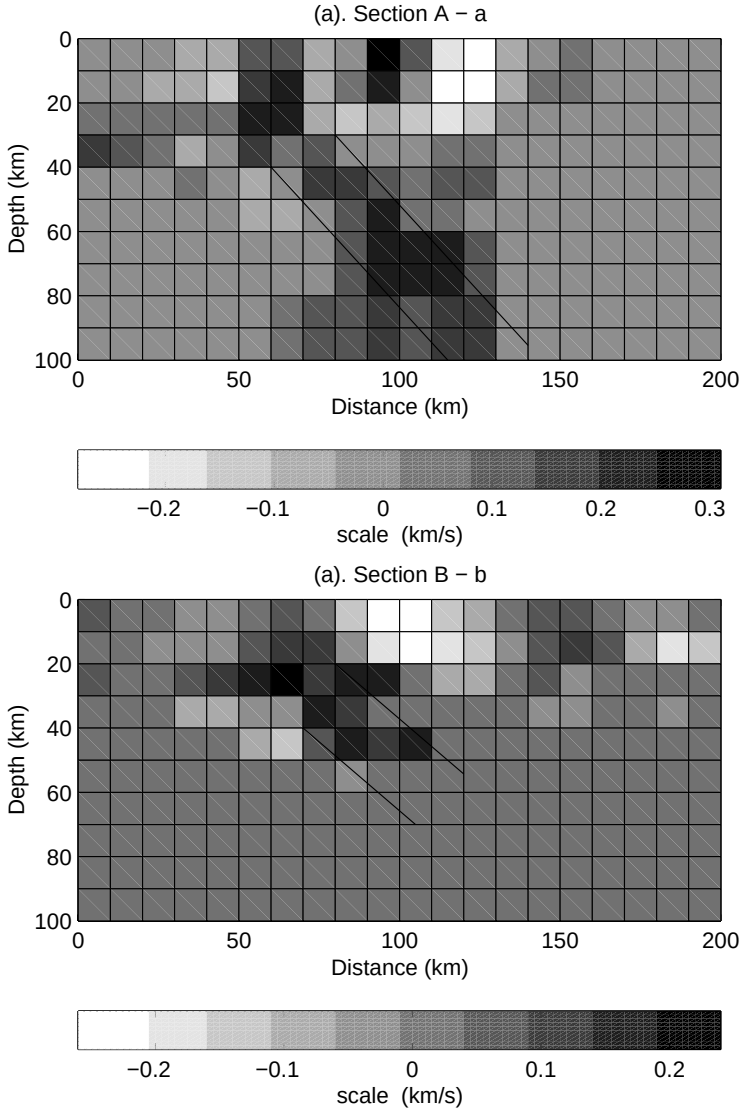

Figure 11. Cross sections (indicated in Figure 1) of P-wave velocity perturbation from the 1D minimum P wave velocity model.

by LSQR together with the Laplacian of the slowness field as the regularization was originally written by Benz and has been applied to several case studies (e.g., Benz et al., 1996). We compared our results shown above with that from LSQR and found the main structures are well matched. Figure 9 is the P wave perturbation image in the first layer produced by LSQR, which has the same pattern as that of Figure 7(a). The only significant difference is that Figure 7(a) gives higher resolution for both positive and negative velocity perturbations in the central part of area. This is because in our inverse algorithm the constraints on the velocity model parameters depend on the ray coverage information, i.e., in areas more densely sampled by the rays, the constraints are looser, while in LSQR we used the model parameters constrained by the Laplacian with a constant weighting factor everywhere. Therefore, we believe that the results presented in this study are essentially inversion algorithm independent. There are several possible explanations for the differences of results when compared to those with of Protti et al. (1996). First of all, the data selection was not the same. We used a much larger data set than that used by Protti et al. Because of this, even though

our study covers a larger geographical area, we have more information on the crustal structure. Secondly, the area studied by Protti et al. is included in our study area and located towards the center of the model. Therefore, our ray coverage is better in the central part of our model and the area corresponding to their study is better resolved in our study.

Acknowledgements

We thank two anonymous referees for their valuable comments and suggestions. We are greatful to OVSICORI-UNA for allowing us to use the data recorded by their seismographic network and A. Tryggvason for fruitful discussions about the forward calculation. The work was supported by Uppsala University.

References

Alvarado, G. E., Barquero, R., Boschini, I., Chiesa, S. and Carr, M. J., 1986, Relacion entre la neotectonica y el vulcanismo en Costa Rica, *Proc. Int. Symp. Neotectonics and Volcanic Hazards*, Bogota, Colombia (in Spanish with English abstract).

Ammon, C. J. and Vidale, J. E., 1993, Tomography without rays, *Bull. Seism. Soc. Am.* **83**, 509–528.

Astorga, A., Fernandez, J. A., Barboza, G., Campos, L. Obando, J., Aguilar, A. and Obanso, L. G., 1991, Cusencas sedimentarias de Costa Rica: evolucion geo-dinamica y potencial de hidrocaburos, *Rev. Geol. America Central* **13**, 25–29 (in Spanish with English abstract).

Barquero, R. and Rojas, W., 1994, Sismicidad inducida por el terremoto de Limon, *Rev. Geol. America Central*, Vol. esp. Terremoto de Limon, pp. 111–120 (in Spanish with English abstract).

Benz, H., Zandt, G. and Oppenheimer, D. H., 1992, Lithospheric structure of northern California from teleseismic images of the upper mantle, *J. Geophys. Res.* **97**, 4791–4807.

Benz, H., Chouet, B. A., Dawson, P. B., Lahr, J. C. and Page, R. A., 1996, Three-dimensional P and S wave velocity structure of Redoubt Volcano, Alaska, *J. Geophys. Res.* **101**, 8111–8128.

Benz, H. M. and Smith, R. B., 1984, Simultaneous inversion for lateral velocity variations and hypocenters in the Yellowstone region using earthquake and refraction data, *J. Geophys. Res.* **89**, 1208–1220.

Berryman, J. G., 1990, Lecture notes on nonlinear inversion and tomography, Lawrence Livermore, Natl. Lab. Rep., UCRL-LR-105358.

Crosson, R., 1976, Crustal structure modeling of earthquake data. i. Simultaneous least squares estimation of hypocenter and velocity parameters, *J. Geophys. Res.* **81**, 3036–3046.

De Jonge, M. R., Wortel, M. J. R. and Spakman, W., 1993, From tectonic reconstruction to upper mantle model: an application to the Alpine-Mediterranean region, *Tectonophysics* **223**, 53–65.

DeMets, C., Gordon, R. G., Argus, D. F. and Stein, S., 1990, Current plate motions, *Geophys. J. Int.* **101**, 425–478.

Escalante, G. and Astorga, A., 1994, Geologia del este de Costa Rica y el norte de Panama, *Rev. Geol. America Central*, Vol. esp. Terremoto de Limon, pp. 1–14 (in Spanish with English abstract).

Hanke, M. and Hansen, P. C., 1994, Regularization methods for large-scale problems, *Surveys on Mathematics for Industry* **3**, 253–315.

Hole, J. A., 1992, Nonlinear high-resolution three-dimensional seismic travel time tomography, *J. Geophys. Res.* **97**, 6553–6562.

Isacks, B. L. and Barazangi, M., 1977, Geometry of Benioff zones: lateral segmentation and downwards bending of the subducted lithosphere. In: Talwani, M. and Cpitman III, W. (eds), *Island-Arcs, Deep Sea Trenches, and Back-Arc Basins*, Maurice Ewing Ser., Vol. 1, Am. Geophys. Union, Washington, DC, pp. 99–114.

Kissling, E., Ellsworth, E., Eberhart-phillips, W. L. and Cockerham, R., 1984, Three-dimensional structure of the Long Valley Caldera, California, region by geotomography, U.S. geol. Surv. Open File Rep., 84-939, pp. 188–220.

Kissling, E., 1988, Geotomography with local earthquake data, *Rev. Geophys.* **26**, 659–698.

Kissling, E., Ellsworth, E., Eberhart-phillips, W. L. and Krudolfer, U., 1994, Initial reference models in local earthquake tomography, *J. Geophys. Res.* **81**, 3036–3046.

Klein, F. W., 1978, Hypocenter location program Hypoinverse, U. S. Geol. Surv. Open-File Rept. 78-694.

Klein, F. W., 1984. User's guide to hypocenters, a program for Vax and Pc 350 computers to solve for earthquake locations, U. S. Geol. Surv. Open-File Rept. 84-000.

Lees, J. M. and Crosson, R. S., 1989, Tomographic inversion for three-dimensional velocity structure at Mount St. Helens using earthquake data, *J. Geophys. Res.* **94**, 5716–5728.

Liaw, H. B., 1981, Seismic velocity modeling from an ensemble of earthquales, PhD Thesis, University of Texas, Dallas.

Ludington, S., Castillo, R. and Azuola, H., 1987, Geology of Costa Rica, in mineral resources assessment of the Republic of Costa Rica, U.S. Geol. Surv. Misc. Invest., Map I-1865, pp. 6–7.

Matumoto, T., Othake, M., Latham, G. and Umana, J., 1977, Crustal structure of southern Central America, *Bull. Seism. Soc. Am.* **67**, 121–134.

Montero, W. P. & Dewey, J. W., 1982, Shallow-focus seismicity, composite focal mechanism, and tectonics of the Valle Central of Costa Rica, *Bull. Seism. Soc. Am.* **72**, 1611–1626.

Micheal, A. J., 1988, Effects of three-dimensional velocity structure on the seismicity of the 1984 Morgen Hill, California, aftershock sequence, *Bull. Seism. Soc. Am.* **78**, 1199–1221.

Pavlis, L. and Booker, J. R., 1980, The mixed discrete-continuous inverse problem: application to the simultaneous determination of earthquake hypocenters and velocity structure, *J. Geophys. Res.* **85**, 4801–4810.

Podvin, P. and Lecomte, I., 1991, Finite difference computation of travel-times in very contrasted velocity models: A massively parallel approach and its associated tools, *Geophys. J. Int.* **105**, 271–284.

Ponce, D. A. and Case, J. E., 1987, Geophysical interpretation of Costa Rica, in Mineral resources assessment of the Republic of Costa Rica, U.S. Geol. Surv. Misc. Inverst. Folio, I-1865, pp. 8–17.

Protti, M., McNally, K. and Guendel, F., 1994, The geometry of the Wadati-Benioff zone under southern Central America and its tectonic significance: results from a high-resolution local seismographic network, *Phys. Earth. Planet. Interiors* **84**, 271–287.

Protti, M., Schwartz, S. Y. and Zandt, G., 1996, Simultaneous inversion for earthquake location and velocity structure beneath central Costa Rica, *Bull. Seism. Soc. Am.* **86**, 19–31.

Quintero, R., Osypov, K., Kulhanek, O., 1997, Crustal structure below Costa Rica, Abstracts of the 29th General Assembly of the International Association of Seismology and Physics of the Earth Interior, Thessaloniki, Greece, 18–28, August 1997, p. 213.

Spakman, W., 1993, Iterative strategies for non-linear travel time tomography using global earthquake data. In: Iyer, H. M. and Hirahara, K. (eds), *Seismic Tomography: Theory and Practice*, Chapman and Hall.

Rivier, S. F., 1985, Seccion geologica del Pacifico al Atlantico a traves de Costa Rica, *Rev. Geol. Am. Central* **2**, 23–32.

Tarantola, A., 1987, *Inverse Problem Theory*, Elsevier.

Tarantola, A. and Valette, B., 1982, Generalized nonlinear inverse problem solved using least squares criterion, *Rev. Geophys. Space phys.* **20**, 219–232.

Thurber, C. H., 1984, Seismic detection of the summit magma complex of Kilauea Volcano, Hawaii, *Science* **223**, 165–167.

Van der Hilst, R. D. and Spakman, W., 1989, Importance of the reference model in linearized tomography and images of subduction below the Caribbean plate, *Geophys. Rev. Lett.* **16**, 1093–1096.

Van der Hilst, R. D., Engdahl, R., Spakman, W. and Nolet, G., 1991, tomographic imaging of subducted lithosphere below northwest Pacific island arcs, *Nature* **353**, 37–43.

Vidale, J. E., 1988, Finite-difference calculations of traveltimes, *Bull. Seismol. Soc. Am.* **78**, 2062–2076.

Vidale, J. E., 1991, Finite-difference calculations of traveltimes in three dimensions, *Geophysics* **55**, 2062–2076.

Yanick, R., 1996, The three-dimentional seismological model a priori constrained: Confrontation with seismic data, *J. Geophys. Res.* **101**, 8457–8472.

Yao, Z., Osypov, K. and Roberts, R., 1998, Travel-time tomography using regularized recursive least squares, *Geophys. J. Int.* **134**, 545–553.

Zhao, D., Hasegawa, A. and Horiuchi, S., 1992, Tomographic imaging of P and S wave velocity structure beneath northeastern Japan, *J. Geophys. Res.* **97**, 19909–19928.

Zhou, H. and Clayton, R. W., 1990, P and W wave travel time inversions for subducting slab under the island arcs of the northwest Pacific, *J. Geophys. Res.* **95**, 6829–6851.